Chinese Journal of Catalysis 35 (2014) 748–756

available at www.sciencedirect.com

ScienceDirect

journal homepage: www.elsevier.com/locate/chnjc

Article (Special Issue on the 2nd International Congress on Catalysis for Biorefineries (CatBior 2013))

Hydrodeoxygenation of palm oil to hydrocarbon fuels over Ni/SAPO-11 catalysts

Qiying Liu, Hualiang Zuo, Qi Zhang, Tiejun Wang *, Longlong Ma #

CAS Key Laboratory of Renewable Energy, Guangzhou Institute of Energy Conversion, Chinese Academy of Sciences, Guangzhou 510640, Guangdong, China

ARTICLE INFO

Article history:
Received 22 August 2013
Accepted 12 September 2013
Published 20 May 2014

Keywords:
Palm oil
Hydrodeoxygenation
Hydrocarbon
Isomerization
Synergistic effect

ABSTRACT

Small particles of SAPO-11 with large surface area and mesoporosity were synthesized hydrothermally. Ni/SAPO-11 catalysts with different Ni loadings were prepared by incipient wetness impregnation, and their physicochemical properties were characterized by X-ray diffraction, scanning electron microscopy, N_2 adsorption-desorption, NH_3 temperature-programmed desorption, Thermogravimetric, and H_2 chemisorption. In the Ni impregnation of SAPO-11, the mesopores of SAPO-11 accommodated the Ni particles and give good dispersions, but with the partial blocking of some micropores. In the hydrodeoxygenation of palm oil, the production of liquid alkanes depends on the competition between hydrodeoxygenation and decarbonylation pathways via the corresponding carboxylic acid intermediates. The weak and medium acidity of SAPO-11 and a good match of the Ni and SAPO-11 functions in the Ni/SAPO-11 catalysts decreased the cracking of primary long chain alkanes and gave a high liquid alkane yield of 70 wt% and isomerization selectivity of >80 mol%.

1. Introduction

Vegetable oil contained in biomass is a vast and easily available renewable carbon resource. Using vegetable oil as the feedstock to produce green fuels for substituting nonrenewable fossil energy has received more attention in the last decade due to increasing concerns over environmental problems induced by burning fossil fuels [1,2]. Catalytic hydrodeoxygenation (HDO) of vegetable oil to hydrocarbon fuels has obvious advantages as compared to their transesterification with methanol because oxygen removal and saturation of C=C bonds during HDO processing result in hydrocarbon fuels with desirable transportation fuel properties such as high heating value, chemical stability, and low freezing point [3,4].

Sulfided W and Mo modified with Ni and Co catalysts were used for obtaining high alkane yields in the HDO of vegetable oil to hydrocarbon fuels. However, sulfur containing reagents are necessary to maintain the catalytic activity and stability during the pretreatment of catalysts and HDO processing, which inevitably causes sulfur contamination of the final products [5–7]. Noble metals including Pt and Pd were also employed to produce hydrocarbon fuel in the diesel range [8,9], but the exorbitant costs limit their applications on a large scale. Recently, metal carbides and phosphides were investigated and high yields of liquid hydrocarbon were obtained. However, the preparation procedures for these catalysts were tedious, and

* Corresponding author. Tel: +86-20-87057751; Fax: +86-20-87057737; E-mail: wangtj@ms.giec.ac.cn
# Corresponding author. Tel/Fax: +86-20-87057673; E-mail: mall@ms.giec.ac.cn
This work was supported by the National Basic Research Program of China (973 Program, 2012CB215304), the Natural Scientific Foundation of Guangdong Province (S2012040006992), and the National Natural Science Foundation of China (51376185 and 51161140331).
DOI: 10.1016/S1872-2067(12)60710-4 | http://www.sciencedirect.com/science/journal/18722067 | Chin. J. Catal., Vol. 35, No. 5, May 2014

change in the active phase was observed during the HDO of vegetable oils, leading to the limited lifetimes of these catalysts [10–12].

In addition, the acid-base properties of the support play an essential role in mediating the product distribution in the HDO of vegetable oil. For example, with basic MgO as the catalyst, heavy alkanes with carbon number larger than 35 were mainly manufactured due to C–C coupling of fatty ester intermediates [13]. In comparison, supports with the appropriate acidity significantly promoted liquid hydrocarbon production by enhancing dehydration/hydrogenation of the alcohol intermediates, but supports with strong acidity cause severe cracking to lighter hydrocarbons [14].

A drawback of the hydrocarbons produced by the HDO of vegetable oil is their poor low temperature properties because the freezing points of *n*-alkanes with long carbon chains are higher than 273 K, and they are unsuitable for cold areas. This problem can be solved by hydro-isomerization of the *n*-alkanes using noble metals supported on acidic zeolite catalysts [15]. However, for good economics and process efficiency, a one-step production of isomerized hydrocarbons by coupling HDO processing and the isomerization of long *n*-alkanes in one reactor is desirable.

SAPO zeolites synthesized by replacing framework Al with Si possess different pore structures with a wide range of pore sizes. They are important members in the family of aluminophosphate molecular sieves. SAPOs mainly have weak and medium acidity from the Si doping and they have shown promising applications in many acid-catalyzed reactions [16,17]. High selectivity in the hydroisomerization of long *n*-alkanes was observed with noble metal Pt and Pd supported on SAPOs as bifunctional catalysts [18]. Owing to their intrinsic acidity and pore structures, SAPOs would be good supports for producing isomerized hydrocarbon in the HDO of vegetable oils. However, the investigation of this was seldom [19,20]. Recently, we compared the catalytic performance of Ni supported on different commercial supports in the HDO of methyl hexadecanoate in an autoclave, in which it was found that a Ni/SAPO-11 catalyst with weak and medium acidity showed > 95% liquid alkane yield with very low isomerization selectivity [21].

In this work, we hydrothermally synthesized SAPO-11 as small particles with large surface area and mesoporosity. Ni/SAPO-11 catalysts were prepared by incipient wetness impregnation, and their catalytic performance was tested in a one-step HDO of palm oil to isomerized hydrocarbons. The catalysts were characterized by X-ray diffraction (XRD), scanning electron microscopy (SEM), N_2 adsorption-desorption, NH_3 temperature-programmed desorption (NH_3-TPD), Thermogravimetric (TG), and H_2 chemisorption. The relation between the acid and metal functions of the catalysts and HDO performance was elucidated, and the HDO reaction pathway was discussed.

2. Experimental

2.1. Catalyst preparation

According to the previous report [22], SAPO-11 can be hydrothermally synthesized without using a surfactant. H_3PO_4 (85% of aqueous solution, 26.0 g) and pseudo-boehmite (27.1 g) were dissolved in 124.5 g H_2O and stirred for 90 min. Then 6.5 g tetrapropyloxysilane (TPOS) and 35.1 g *n*-propanol were added, and the mixture was further stirred for 120 min, followed by dropwise addition of an aqueous solution of 23.7 g di-*n*-propylamine to form a homogeneous sol with the molar ratio of H_3PO_4:Al_2O_3·*n*H_2O:TPOS:di-*n*-propylamine:*n*-propanol:H_2O of 0.226:0.225:0.0246:0.235:0.585:6.917. The sol was transferred to a hydrothermal autoclave (100 mL) lined with Teflon and heated at 458 K for 24 h. The solid product was dried at 393 K and calcined at 873 K for 6 h to obtain the SAPO-11.

The Ni/SAPO-11 catalysts were prepared by impregnating the catalyst support with an aqueous solution of $Ni(NO_3)_2·6H_2O$ with Ni loadings of 2%–9% by weight. The resulting suspension was stirred for 10 h at ambient temperature, followed by evaporating excess water at 353 K. The solid that remained was dried at 393 K and calcined at 823 K for 3 h in air.

2.2. Catalyst characterization

XRD patterns of catalyst were obtained with a X'pert PRO MPD diffraction instrument (PANalytical) operated at 40 kV and 40 mA with Cu K_α (λ = 0.15406 nm) radiation. SEM images of the catalysts were recorded using an S-4800 instrument operated at 2.0 kV. BET surface area and pore size distribution were determined by isothermal adsorption of N_2 at 77 K using a Micromeritics ASAP-2010 automated system. NH_3-TPD experiments were carried out on a homemade instrument equipped with a thermal conductivity detector (TCD). TG analysis of the spent catalyst was performed on a NETZSCH-STA 409PC DSC-SP Thermal analyzer by increasing the temperature from 313 to 1073 K at 10 K/min under air (30 mL/min). H_2 chemisorption measurements were performed on a Quantachrome-ASIQACIV200-2 automated gas sorption analyzer. The catalysts were reduced at 773 K for 2 h with H_2 and further heated at 823 K for 0.5 h under He, followed by cooling down to 323 K for H_2 chemisorption tests. The dispersion of Ni was estimated from the molar ratio of surface metallic Ni to initially introduced Ni species, assuming that one H atom is adsorbed on one Ni atom and no dissolution of H takes place in the Ni particles.

2.3. HDO of palm oil composition

The palm oil (> 99%) was commercially obtained from Yihai (Guangzhou) Food & Oil Industrial Co., Ltd and used without further treatment. The components of the palm oil were determined by transesterification using an alkaline catalyst. Methanol and palm oil with the molar ratio of 6:1 were mixed with KOH in a batch reactor, and the reaction was performed at 338 K for 2 h. After reaction, the supernatant liquid was separated off and washed with distilled water. The methyl esters were diluted with cyclohexane and analyzed on a gas chromatograph (Shimadzu GC-2010) with an FID and a capillary

Table 1
Fatty acid composition of the palm oil.

Fatty acid	Structure	Formula	Composition (mol %)
Myristic acid	$C_{14:0}$	$C_{14}H_{28}O_2$	2.31
Palmitic acid	$C_{16:0}$	$C_{16}H_{32}O_2$	44.23
Stearic acid	$C_{18:0}$	$C_{18}H_{36}O_2$	3.63
Oleic acid	$C_{18:1}$	$C_{18}H_{34}O_2$	41.06
Linoleic acid	$C_{18:2}$	$C_{18}H_{32}O_2$	8.36
Linolenic acid	$C_{18:3}$	$C_{18}H_{30}O_2$	0.12

column (DB-1 HT, 30 m × 0.25 mm × 0.1 μm) using *n*-heptadecane as internal standard. The composition of the palm oil is listed in Table 1.

The HDO of the palm oil was performed on a fixed-bed reactor at high pressure. Before reaction, 2.0 g (3 mL) catalyst (40–60 mesh) was loaded into a tubular stainless steel reactor with the inner diameter of 10 mm and the length of 300 mm, and reduced at 773 K for 2 h by a high purity H_2 (99.999%) flow. After the system was cooled to the reaction temperature, palm oil was fed in at 0.05 mL/min by a syringe pump and mixed with the high purity H_2 of 50 mL/min. Then the gas-liquid mixture was introduced into the reactor using a preheater at 473 K at the LHSV of 1.0 h^{-1} and H_2 pressure of 4.0 MPa. The reaction temperature was measured by a thermocouple in the catalyst bed and controlled by a temperature controller. The system pressure was controlled by a backpressure regulator. The gas was collected by a sampling bag placed after a condenser and a gas-liquid separator. The liquid products including unconverted palm oil were obtained by collecting the upper oil phase of the two-phase oil-water liquid from an oil-water separator.

C_1–C_4 hydrocarbons were analyzed by a GC 9800 chromatograph equipped with an FID and a packed column (Porapak-Q column, 3 m × 3 mm) using N_2 as the carrier gas. CO, CO_2, and CH_4 were analyzed by another GC 9800 equipped with a TCD and a packed column (TDX-01 column, 3 m × 3 mm) using He as the carrier gas. The gaseous products were quantified by the external standard method using CH_4 as the standard. The liquid products were diluted with cyclohexane, identified by GC-MS measurement, and quantified by an Agilent Tecnologies 4890 gas chromatograph equipped with an FID and a capillary column (DB-1701, 60 m × 0.25 mm × 0.25 μm) using n-nonadecane as the internal standard. The experimental error of the GC measurements was ±5%.

Yield of liquid hydrocarbons (Y) and selectivity of product i (S_i, mol%) were defined as:

$$Y = m_l/\Delta m \times 100\%$$

$$S_i = n_i \times a_i/(\sum_1^i n_i \times a_i) \times 100\%$$

Here, Δm is the weight of palm oil fed in, m_l means the weight of liquid hydrocarbons calculated by GC analysis, n_i indicates the moles of product i, and a_i represents the carbon atom number of product i.

Assuming the same calibration factor for the normal and branched alkane isomers in the GC measurement, the selectivity of isomerized liquid alkane was determined by

$$S_{iso} = \sum_1^i (A_i/M_i) \,/\, \sum_1^i (A_i/M_i + A_n/M_n) \times 100\%$$

A_i and M_i are the peak areas of isomerized alkane product i in GC analysis and its molecular weight, respectively. A_n and M_n indicate the peak area of normal alkane product i and its molecular weight.

3. Results and discussion

3.1. HDO of palm oil

Palm oil contains mainly palmitic and oleic fatty chains (total amount > 85%) with small amounts of myristic, stearic, linoleic, and linolenic fatty chains (Table 1). Its acid value and water content were measured as less than 0.12 and 0.3 mg/g, respectively, indicating trace amounts of free carboxylic acid and H_2O in the palm oil.

Table 2 shows the catalytic performance of Ni/SAPO-11 with different Ni loadings in the HDO of palm oil. At the Ni loading of 2 wt%, the liquid alkane yield of C_5–C_{18} was 60 wt% with the isomerized selectivity of 46%. Among the liquid alkanes, the selectivities to C_5–C_{14} and C_{15}–C_{18} chains were 18.7% and 70%, respectively, indicating that some cracking of long chain alkanes took place. In addition, gaseous CO and C_1–C_4 alkanes were detected with a total amount of 10.9%. As the Ni loading was increased to 7 wt%, the liquid alkane yield and isomerized selectivity were significantly increased to 67.4% and 61.5%, respectively. As the Ni loading was further increased to 9 wt%, the liquid alkane yield was similar, but the C_5–C_{14} and C_1–C_4 alkanes increased obviously because primary long chain alkanes were susceptible to cracking to lighter compounds [23]. The production of isomerized alkanes depends on the formation of carbenium ions from the primary n-alkanes on the acidic SAPO-11 and the skeletal rearrangement and propagation of the carbenium ions over metallic Ni centers [18]. The high isomerization selectivity of >83% in this case indicated that a good balance between the metal Ni and

Table 2
HDO of palm oil over Ni/SAPO-11 catalysts with different Ni loadings.

Catalyst	Product distribution (C mol%)									Yield of liquid alkane (wt%)
	CO	CO_2	C_1–C_4	C_5–C_{14}		C_{15}–C_{18}		Liquid alkane		
				i [a]	n [b]	i	n	i	n	
2 wt%Ni/SAPO-11	1.4	0.0	9.5	12.9	5.8	28.0	42.0	46.2	53.8	60.0
5 wt%Ni/SAPO-11	1.3	0.0	9.4	10.2	6.8	37.7	34.1	54.0	46.0	60.4
7 wt%Ni/SAPO-11	1.7	0.0	10.0	7.7	5.7	46.8	28.5	61.5	38.5	67.4
9 wt%Ni/SAPO-11	1.1	0.0	14.1	26.2	9.2	44.2	4.8	83.4	16.6	67.9

Reaction conditions: catalyst 2 g, 633 K, H_2 pressure 4.0 MPa, TOS = 6.0 h, LHSV = 1.0 h^{-1}.

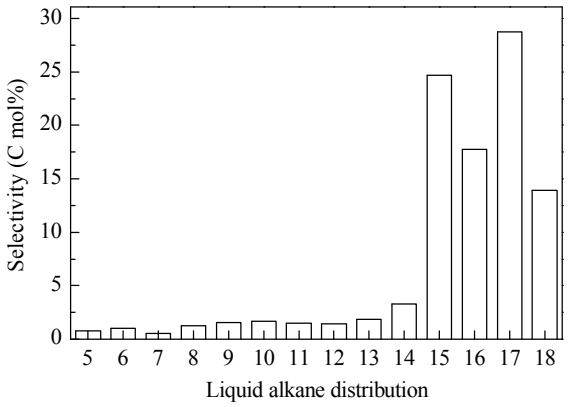

Fig. 1. Liquid alkane distribution over 7 wt%Ni/SAPO-11 under the same reaction condition as Table 2.

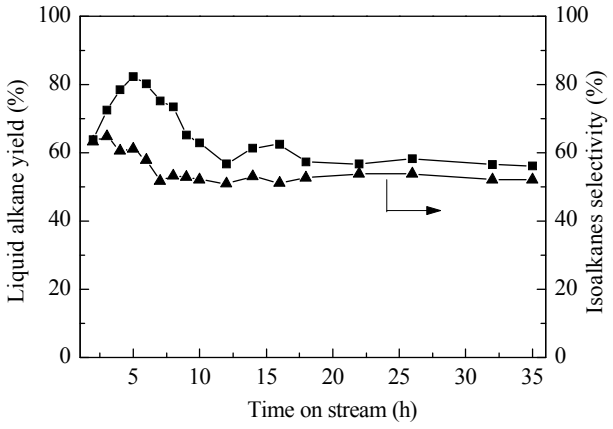

Fig. 2. Stability test of 7 wt%Ni/SAPO-11 in the HDO of palm oil. Reaction conditions: 633 K, H_2 pressure 4.0 MPa, LHSV = 1.0 h^{-1}.

acid SAPO-11 functions was reached with the 9 wt%Ni/SAPO-11 catalyst. A typical liquid alkane distribution in the HDO of palm oil is shown in Fig. 1. More than 85% of the liquid alkanes were C_{15}–C_{18}, indicating that the cracking of long alkanes was significantly suppressed.

Considering that the 7 wt%Ni/SAPO-11 showed a high liquid alkane yield and significantly suppressed cracking selectivity, the influence of the reaction temperature was further investigated in the HDO of palm oil with this catalyst. The results are presented in Table 3. At the low reaction temperature of 593 K, the liquid alkane yield and isomerized selectivity were 43.8% and 35%, respectively. The selectivity of the primary C_{15}–C_{18} alkanes was 85.1% with the cracked C_5–C_{14} alkane selectivity of 8% and the gaseous C_1–C_4 alkane selectivity of 4.4%. As the temperature increased to 633 K, the liquid alkane yield and the isomerized selectivity gradually increased for the liquid C_5–C_{14} fraction and that of the gaseous C_1–C_4 alkanes slightly increased at the expense of the C_{15}–C_{18} alkanes. As the reaction temperatures were further increased to 653 and 673 K, the liquid alkane yields changed a little, but the isomerized selectivities were significantly increased to above 80%. Meanwhile, both the gaseous C_1–C_4 and the liquid C_5–C_{14} alkanes were sharply increased due to the significant cracking of the primary C_{15}–C_{18} alkanes at higher temperatures. Therefore, the reaction temperature showed the essential role of mediating the liquid alkane yields, product distribution, and isomerization selectivities.

Figure 2 shows the stability test of 7 wt%Ni/SAPO-11 in the HDO of palm oil at 633 K, H_2 pressure 4.0 MPa, and LHSV = 1.0 h^{-1}. The liquid alkane yield increased from the initial 62% to the maximum of 82% after 5 h, and then gradually decreased and stabilized at 58%. On the other hand, the selectivity to isomerized alkanes monotonically dropped from the initial 62% to the stabilized 52% after 7 h of time on stream. This 58% of liquid alkane yield corresponded to 70% of the maximum possible value based on average molecular weight of palm oil and weight discrepancy due to C=C bond saturation, and oxygen and propane removal. Neither obviously decreased liquid alkane yield nor isomerized selectivity was observed after 35 h of reaction, demonstrating the good stability of the Ni/SAPO-11 catalyst in the HDO of palm oil.

3.2. Catalyst characterization

Figures 3(a) and (b) show the SEM image of SAPO-11 and XRD patterns of SAPO-11 and 7 wt%Ni/SAPO-11, respectively. The SAPO-11 sample was present as cloud-like with very small particles of less than 50 nm. The XRD pattern of pristine SAPO-11 showed a typical AEL structure, indicating that SAPO-11 was successfully synthesized by this hydrothermal method. After the SAPO-11 was impregnated with 7 wt% Ni, the diffraction intensities corresponding to the AEL structure decreased but were largely conserved, indicating that this incipient wetness impregnation did not destroy the crystalline and pore structures of SAPO-11. Apart from those of SAPO-11, diffraction peaks corresponding to NiO (2θ = 37.2°, 43.4°, and 62.8°) were present, indicating that the supported Ni^{2+} species were aggregated into NiO crystallites on the surface of SAPO-11. After 35 h of the stability test, the sizes of the SAPO-11 particles were significantly sintered to 100 nm while

Table 3
HDO of palm oil over 7 wt%Ni/SAPO-11 at different temperatures.

Reaction temperature (K)	Product distribution (C mol%)									Yield of liquid alkane (wt%)
	CO	CO_2	C_1–C_4	C_5–C_{14}		C_{15}–C_{18}		Liquid alkane		
				i	*n*	*i*	*n*	*i*	*n*	
593	2.5	0.0	4.4	4.6	3.4	30.8	54.3	35.0	65.0	43.8
613	2.1	0.0	4.4	2.5	3.4	45.3	36.8	54.3	45.7	62.1
633	1.7	0.0	10.0	7.7	5.7	46.8	28.5	61.5	38.5	67.4
653	1.6	0.5	8.0	31.8	7.9	43.3	6.7	83.8	16.2	69.3
673	1.2	0.0	17.0	36.2	12.4	29.6	3.4	80.7	19.3	66.1

Reaction conditions see Table 2.

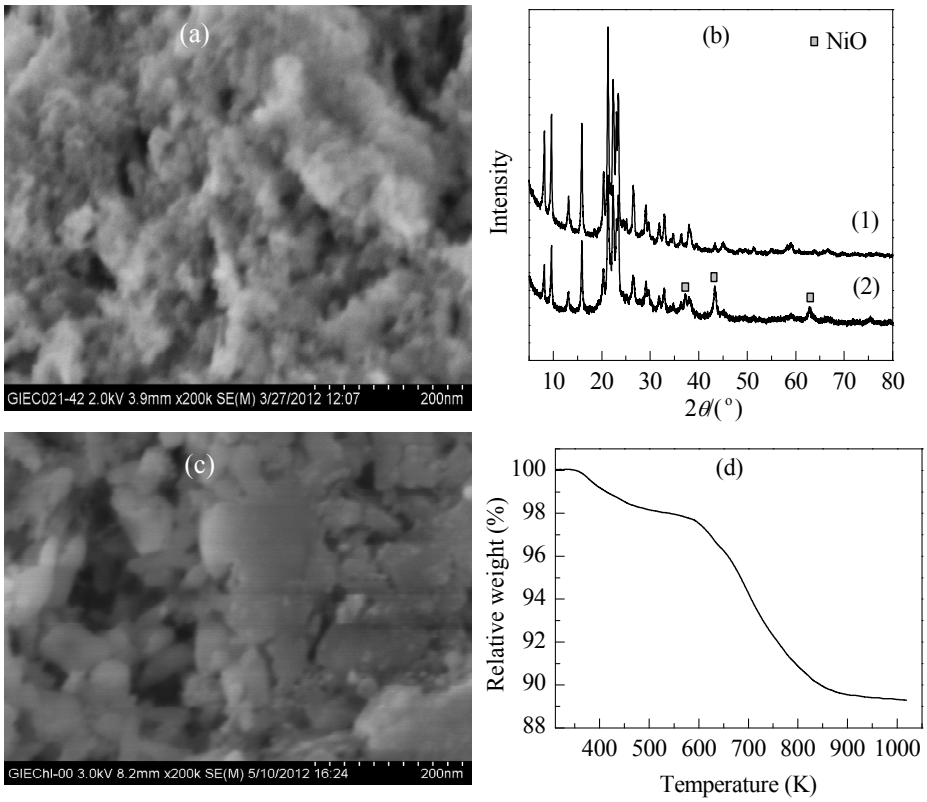

Fig. 3. SEM images of SAPO-11 (a) and spent 7 wt%Ni/SAPO-11 (c), XRD patterns (b) of SAPO-11 (1) and 7 wt%Ni/SAPO-11 (2) and (d) TG profile of spent 7 wt%Ni/SAPO-11.

the Ni particles were less than 20 nm, as indicated by the SEM result (Fig. 3(c)). The TG profile of the spent 7 wt%Ni/SAPO-11 revealed 2% weight loss at 350–550 K and 8.7% weight loss at 550–900 K (Fig. 3(d)). The first weight loss was due to the removal of physically adsorbed water and organic products and the latter one was due to the combustion of deposited carbon on catalyst surface. We propose that the good stability of 7 wt%Ni/SAPO-11 in the HDO of palm oil originated from less carbon deposition due to the fact that the mesopores of the catalyst enhanced the fast diffusion of feedstock and products.

The textural properties of the Ni/SAPO-11 catalysts with different Ni loadings are shown in Table 4. The pristine SAPO-11 support had the BET surface area of 255.5 m^2/g with the external surface of 151.1 m^2/g and mesopore volume of 0.214 cm^3/g. The external surface and mesoporosity were possibly from the nano-sized SAPO-11 particles and their stacking, respectively. Ni loading significantly reduced the BET and external surface area and mesoporosity of the Ni/SAPO-11 catalysts, but these still had the large surface area and mesopore volumes of more than 100 m^2/g and 0.1 cm^3/g, respectively, even at the high Ni loading of 9 wt%. As compared with the loss in interior surface area (surface area determined by BET surface area subtracted from external surface area) in the Ni/SAPO-11 catalysts, the external surface area decreased more. SAPO-11 is a microporous zeolite with ten-membered rings of 0.4 nm × 0.65 nm [24]. This small pore size cannot afford enough space for Ni particles, which results in most Ni species were agglomerated into particles in the mesopores of SAPO-11 even at the low Ni loading. It was highly possible that supported Ni was also located at the pore mouth of SAPO-11 and partial blocked its microchannels, leading to the significant drop in surface area and pore volume. Ni dispersion on the Ni/SAPO-11 catalysts with different Ni loadings were measured by H_2 chemisorption, and their particle sizes were evaluated as in a previous report [25]. The Ni dispersion decreased with increasing Ni loading, and larger Ni particle sizes were obtained at higher Ni loadings. The pore size distribution of Ni/SAPO-11 is shown in Fig. 4. As compared with SAPO-11, a slightly reduced pore size was observed on the 7 wt%Ni/SAPO-11 catalyst. This implied that 7 wt% Ni loading on SAPO-11 did not significantly block its mesopores.

Table 4
Textural properties and chemisorption analysis of Ni/SAPO-11 catalysts.

Catalyst	S_{BET} [a] (m^2/g)	S_{ex} [b] (m^2/g)	V_p [c] (cm^3/g)	D [d] (%)	d [e] (nm)
SAPO-11	255.5	151.1	0.214	—	—
2 wt%NiSAPO-11	210.8	121.6	0.188	13.7	5
5 wt%NiSAPO-11	181.3	95.5	0.141	7.4	11
7 wt%NiSAPO-11	159.4	83.6	0.128	6.9	14
9 wt%NiSAPO-11	114.9	50.7	0.098	3.8	25

[a] Surface area calculated by the BET method.
[b] External surface area calculated from the desorption branch by the BJH method.
[c] Mesopore volume calculated from the desorption branch by the BJH method.
[d] Ni dispersion.
[e] Calculated size of Ni particles.

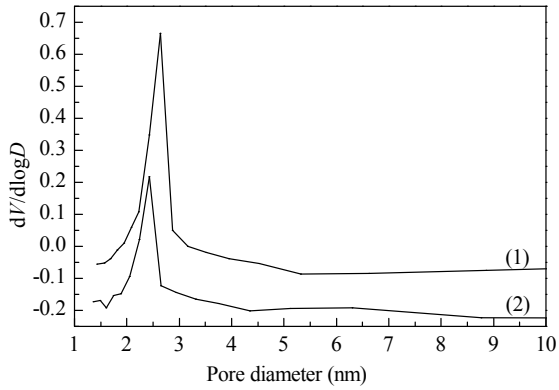

Fig. 4. Pore size distributions of SAPO-11 (1) and 7 wt%Ni/SAPO-11 (2) catalysts.

NH_3-TPD profiles of Ni/SAPO-11 with different Ni loadings are shown in Fig. 5. A main NH_3 desorption peak at 475 K with a weak shoulder at 580 K were observed with the pristine SAPO-11, indicating that weak and medium acidic sites simultaneously existed. Over 2 wt%Ni/SAPO-11, the acidic amounts were nearly unchanged, but the medium acidic sites were increased slightly. As the Ni loading was further increased, both the total and weak acidic sites decreased, but the medium acidic sites slightly increased, which were perhaps created by the supported $Ni^{\delta+}$ species. The weak and medium acidity of the Ni/SAPO-11 catalysts play the essential role of suppressing the cracking of long alkanes to give high yields of liquid alkanes (Table 2, Table 3, and Fig. 1).

3.3. HDO pathway

The HDO of vegetable oils is a complex reaction network comprising the saturation of unsaturated fatty chains, HDO, decarbonylation/decarboxylation, cracking and carbon deposition with carboxylic acids and alcohols as intermediates [26–29]. The unsaturated C=C bonds in palm oil are first hydrogenated to give the saturated triglycerides because of their low energy barrier. Apart from the HDO of saturated palm oil (during this HDO process, palm oil is hydrogenated to fatty acids and then fatty aldehydes, followed by fast hydrogenation to fatty alcohol intermediates [30]) to the alkanes with lengths equal to the corresponding fatty chains, the competitive decarbonylation/decarboxylation of fatty acid intermediates (fatty aldehyde intermediates are produced by decarbonylation and alkanes are obtained from decarboxylation) was observed to occur in parallel to give alkanes with one carbon number less than the pristine fatty chains and CO/CO_2. Both the HDO and decarbonylation pathways proceed by successive hydrogenation, dehydration, and hydrogenation steps. During the transformation of palm oil, hydrogenation and decarbonylation/decarboxylation occur over the metal Ni component in the Ni/SAPO-11 catalysts, while cracking and carbon deposition take place over both Ni and SAPO-11 sites. In addition, the acidic SAPO-11 promotes the dehydration of fatty alcohol intermediates to alkenes, which are further hydrogenated to alkanes and accelerates the total HDO kinetics to give trace amounts of fatty alcohols in the final product (below 0.01%).

In our case, intermediates including myristic, palmitic, and stearic acids were detected. Their yields decreased with increasing reaction temperature (Fig. 6) because the kinetics of the sequential hydrogenation of triglycerides and carbonylation/carboxylation of carboxylic acids were enhanced at higher temperatures. The formation of carboxylic acids occurred by splitting of the ether bonds followed by hydrogenation over our bifunctional Ni/SAPO-11 catalysts (synergistic activation of C–O bond over acidic sites and hydrogenation over metal sites) during hydrogenolysis of palm oil [31], which is consistent with the previous report [27].

The selectivities to gaseous CO and C_1–C_4 alkanes and the molar ratios of C_{15}/C_{16} and C_{17}/C_{18} alkanes were investigated at different reaction temperatures. The results are shown in Fig. 7. As the reaction temperature increased from 593 to 653 K, CO sharply decreased together with significantly increased CH_4 and slightly increased C_2–C_3 alkanes. As the reaction temperature was further increased to 673 K, both CO and CH_4 amounts dropped, with the ethane and propane amounts almost unchanged and butane amount slightly increased. Among these

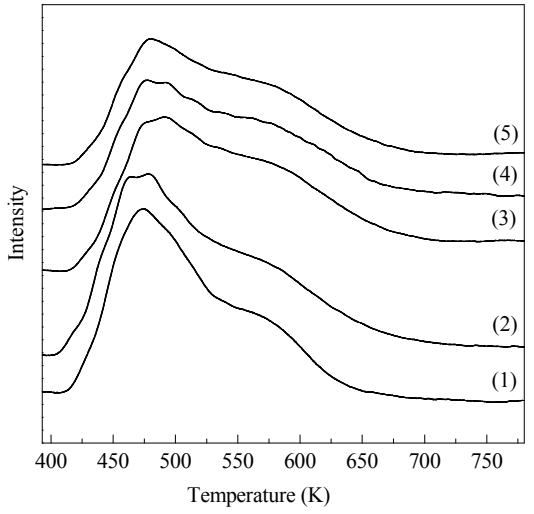

Fig. 5. NH_3-TPD profiles of Ni/SAPO-11 catalysts with different Ni loadings. (1) SAPO-11; (2) 2 wt%Ni/SAPO-11; (3) 5 wt%Ni/SAPO-11; (4) 7 wt%Ni/SAPO-11; (5) 9 wt%Ni/SAPO-11.

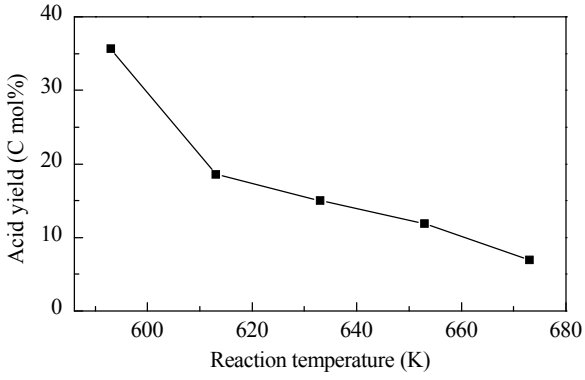

Fig. 6. Carboxylic acid yields in the HDO of palm oil over 7 wt%Ni/SAPO-11 at different reaction temperatures. Reaction conditions: H_2 pressure 4.0 MPa, TOS = 6.0 h, LHSV = 1.0 h^{-1}. The detectable acids include myristic, palmitic, and stearic acids.

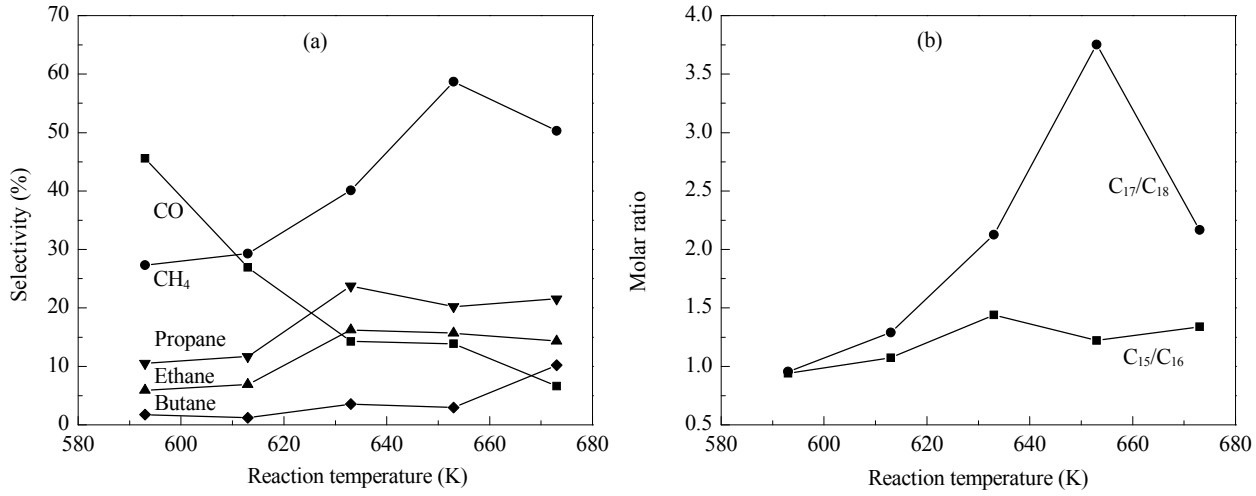

Fig. 7. Gas product selectivities (a) and molar ratios of C_{15}/C_{16} and C_{17}/C_{18} alkanes (b) in the HDO of palm oil over 7 wt%Ni/SAPO-11 catalysts at different reaction temperatures. The reaction conditions see Fig. 6.

products, CH_4 was the majority species at temperatures higher than 633 K mainly due to the methanation of CO originating from the decarbonylaion of carboxylic acid intermediates. Propane produced by the direct hydrogenolysis of palm oil can be further cracked into ethane and CH_4, which are the same products from the splitting of the long alkanes. More important, butane exclusively produced by the cracking of long alkanes was less than 10% in the gas products, demonstrating that heavy cracking of long alkanes was significantly suppressed. Despite that no pentadecanoic and heptadecanoic acids were observed in the palm oil (Table 1), C_{15} and C_{17} alkanes were detected in significant amounts in the liquid products and the molar ratios of C_{15}/C_{16} and C_{17}/C_{18} increased while the ratios of C_{17}/C_{18} increased more remarkably as the reaction temperature increased. This implied that a higher reaction temperature facilitated the decarbonylation of carboxylic acid intermediates and the decarbonylation of stearic acid was easier than that of palmitic acid, possibly due to its longer carbon chain [32]. The lower ratio of C_{17}/C_{18} observed at 673 K was due to the enhanced cracking kinetics of alkanes with long chains. The trends of the gas products and the molar ratio of C_{17}/C_{18} and C_{15}/C_{16} alkanes with reaction temperatures were similar for different times on stream (Fig. 8).

The Ni/SAPO-11 catalysts in this work allowed the HDO of palm oil to proceed along the carboxylic acid pathway and gave nearly 70 wt% liquid hydrocarbon yield. This was due to that the weak and medium acidity of the SAPO-11 support effectively suppressed the cracking of primary long chain alkanes, which gave high stability [14]. In addition, the acidic property of the Ni/SAPO-11 catalysts promoted the isomerization of long alkanes, giving the isomerization selectivity of > 80%. This was significantly superior to those in previous reports where < 20% isomerization selectivities were obtained over sulfided Ni-Mo/Al_2O_3 and Ni/Hβ in the HDO of jatropha and microalgae oils [10,27].

4. Conclusions

SAPO-11 with a large surface area and mesoporosity was hydrothermally synthesized. Ni/SAPO-11 catalysts with different Ni loadings were prepared by incipient wetness impregnation. During Ni impregnation on SAPO-11, the mesopores of

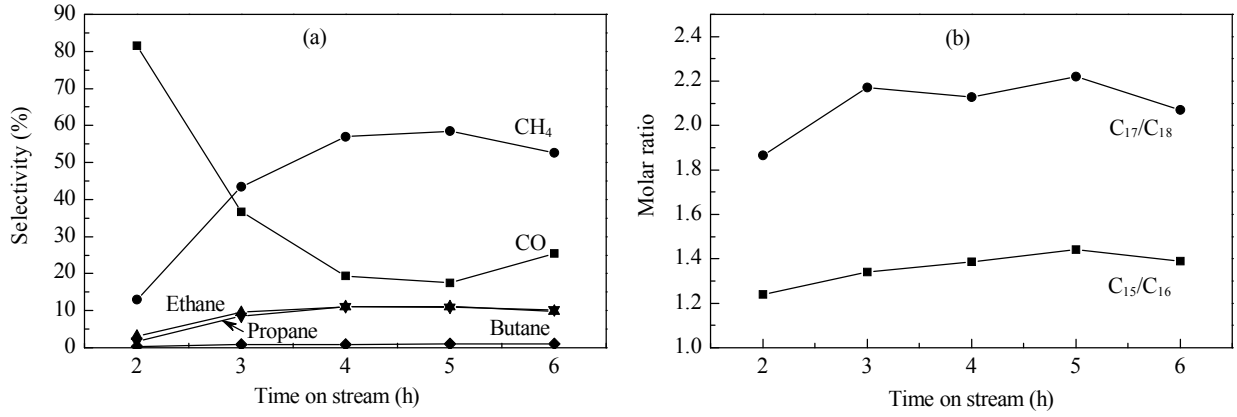

Fig. 8. Gas product selectivities (a) and molar ratios of C_{15}/C_{16} and C_{17}/C_{18} alkanes (b) in the HDO of palm oil over 7 wt%Ni/SAPO-11 up to TOS of 6 h. The reaction conditions were the same as Fig. 2.

Graphical Abstract

Chin. J. Catal., 2013, 34: 748–756 doi: 10.1016/S1872-2067(12)60710-4

Hydrodeoxygenation of palm oil to hydrocarbon fuels over Ni/SAPO-11 catalysts

Qiying Liu, Hualiang Zuo, Qi Zhang, Tiejun Wang *, Longlong Ma *
Guangzhou Institute of Energy Conversion, Chinese Academy of Sciences

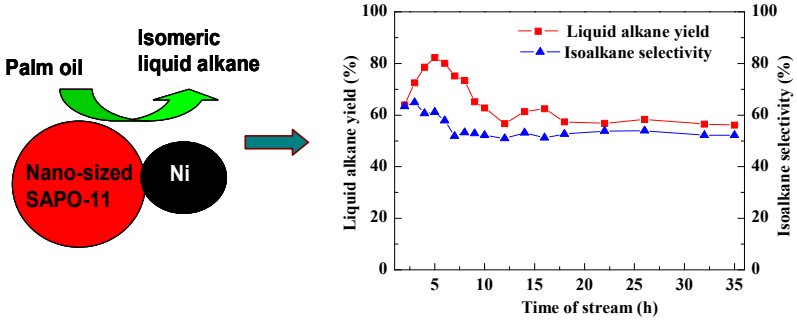

A bifunctional Ni/SAPO-11 catalyst with weak and medium acidities gave high yields of liquid hydrocarbons, > 50% isomerization selectivity, and good stability in the one-step HDO of palm oil.

SAPO-11 could accommodate Ni particles to give good dispersions that depended on Ni loading, but partly blocked its micropores due to that the one dimensional micropores of SAPO-11 do not afford enough space for Ni particles. The transformation of palm oil showed that the production of hydrocarbons depended on parallel HDO and decarbonylation pathways via their carboxylic acid intermediates. Due to the weak and medium acidity and the well matched balance between the metallic Ni and acidic SAPO-11 functions, the Ni/SAPO-11 catalysts significantly suppressed the cracking of long hydrocarbons and gave the high liquid alkane yield of 70% with more than 80% isomerization selectivity and good stability.

References

[1] Agarwal A K. *Prog Energy Combust Sci*, 2007, 33: 233
[2] Smith B, Greenwell H C, Whiting A. *Energy Environ Sci*, 2009, 2: 262
[3] Lotero E, Liu Y, Lopez D E, Suwannakarn K, Bruce D A, Goodwin J G Jr. *Ind Eng Chem Res*, 2005, 44: 5353
[4] Chiappero M, Do P T M, Crossley S, Lobban L L, Resasco D E. *Fuel*, 2011, 90: 1155
[5] Senol O I, Viljava T R, Krause A O I. *Catal Today*, 2005, 100: 331
[6] Kumar R, Rana B S, Tiwari R, Verma D, Kumar R, Joshi R K, Garg M O, Sinha A K. *Green Chem*, 2010, 12: 2232
[7] Guzman A, Torres J E, Prada L P, Nuñez M L. *Catal Today*, 2010, 156: 38
[8] Mäki-Arvela P, Snåre M, Eränen K, Myllyoja J, Murzin D Y. *Fuel*, 2008, 87: 3543
[9] Hancsók J, Krár M, Magyar S, Boda L, Holló A, Kalló D. *Microporous Mesoporous Mater*, 2007, 101: 148
[10] Gong S F, Shinozaki A, Shi M L, Qian E W. *Energy Fuels*, 2012, 26: 2394
[11] Yang Y X, Ochoa-Hernández C, de la Peña O'Shea V A, Coronado J M, Serrano D P. *ACS Catal*, 2012, 2: 592
[12] Han J X, Duan J Z, Chen P, Lou H, Zheng X M, Hong H P. *ChemSusChem*, 2012, 5: 727
[13] Snare M, Kubickova I, Maki-Arvela P, Eranen K, Murzin D Y. *Ind Eng Chem Res*, 2006, 45: 5708
[14] Gong S F, Shinozaki A, Qian E W. *Ind Eng Chem Res*, 2012, 51: 13953
[15] Hancsók J, Krár M, Magyar S, Boda L, Holló A, Kalló D. *Stud Surf Sci Catal*, 2007, 170: 1605
[16] Pastore H O, Coluccia S, Marchese L. *Ann Rev Mater Res*, 2005, 35: 351
[17] Liu G Y, Tian P, Xia Q H, Liu Z M. *J Natur Gas Chem*, 2012, 21: 431
[18] Akhmedov V M, Al-Khowaiter S H. *Catal Rev Sci Eng*, 2007, 49: 33
[19] Kikhtyanin O V, Rubanov A E, Ayupov A B, Echevsky G V. *Fuel*, 2010, 89: 3085
[20] Verma D, Kumar R, Rana B S, Sinha A K. *Energy Eviron Sci*, 2011, 4: 1667
[21] Zuo H L, Liu Q Y, Wang T J, Ma L L, Zhang Q, Zhang Q. *Energy Fuels*, 2012, 26: 3747
[22] Fan Y, Xiao H, Shi G, Liu H Y, Bao X J. *J Catal*, 2012, 285: 251
[23] Elangovan S P, Hartmann M. *J Catal*, 2003, 217: 388
[24] Walendziewski J, Pniak B. *Appl Catal A*, 2003, 250: 39
[25] Takai Y, Ueno A, Kotera Y. *Bull Chem Soc Jpn*, 1983, 56: 2941
[26] Han J X, Sun H, Ding Y Q, Lou H, Zheng X M. *Green Chem*, 2010, 12: 463
[27] Peng B X, Yao Y, Zhao C, Lercher J A. *Angew Chem Int Ed*, 2012, 51: 2072
[28] Senol O I, Ryymin E M, Viljava T R, Krause A O I. *J Mol Catal A*, 2007, 268: 1
[29] de Brimont M R, Dupont C, Daudin A, Geantet C, Raybaud P. *J Catal*, 2012, 286: 153
[30] Ryymin E M, Honkela M L, Viljava T R, Krause A O I. *Appl Catal A*, 2009, 358: 42
[31] Turek T, Trimm D L, Cant N W. *Catal Rev Sci Eng*, 1994, 36: 645
[32] Lestari S, Mäki-Arvela P, Eränen K, Beltramini J, Max Lu G Q, Murzin D Y. *Catal Lett*, 2010, 134: 250